Polar Geosci., **18**, 83–100, 2005

A numerical study of the ocean circulation around the northern Antarctic Peninsula: Barotropic response to tidal forcing

Walter C. Dragani[1,2,4*], Enrique E. D'Onofrio[1,2,3], Jorge O. Speroni[1], Monica E. Fiore[1,2] and Rocío Borjas[1]

[1]*Servicio de Hidrografía Naval and ESCM-INUN, Av. Montes de Oca 2124 (C1270ABV) Ciudad Autónoma de Buenos Aires, Argentina*
[2]*Departamento Ciencias de la Atmósfera y los Océanos, Facultad de Ciencias Exactas y Naturales, Universidad de Buenos Aires, (1428) Ciudad Universitaria, Pabellón II, 2do. piso. Ciudad Autónoma de Buenos Aires, Argentina*
[3]*Instituto de Geodesia, Facultad de Ingeniería, Universidad de Buenos Aires, Av. Las Heras 2214, (1127) Ciudad Autónoma de Buenos Aires, Argentina*
[4]*CONICET, Consejo Nacional de Investigaciones Científicas y Técnicas*
[*]*Corresponding author. E-mail: dragani@hidro.gov.ar*

(Received March 23, 2005; Accepted May 18, 2005)

Abstract: A high-resolution shallow water model was implemented to study tidal propagation around the northern Antarctic Peninsula. Numerical experiments were done using a grid with 3.00′ longitude and 1.05′ latitude resolution. Amplitudes and phases of the four main tidal constituents (M_2, S_2, K_1 and O_1) were used to force the model. Modeled sea levels and currents were compared with observations. The modeled cotidal, corange and tidal ellipse axis obtained by harmonic analysis from model results are in good agreement with those of available observations. Given the good correspondence between harmonic constants obtained from model results and from observed hourly sea levels, the energy flux and dissipation by bottom friction were computed. The most intense energy fluxes are related to the semidiurnal constituents. The highest values are present in the Weddell Sea and the energy flux shows a relative maximum at the Antarctic Strait, flowing from the Weddell Sea to Bransfield Strait. Nearly all the dissipation occurs in the Antarctic Strait (maximum value ~0.25 Wm^{-2}) and around the South Shetland Islands. The total tidal energy lost to bottom friction in our 4-constituent model is about 1.5 GW, giving a domain-averaged value of ~0.002 Wm^{-2}.

key words: numerical model, tide, ocean circulation, Antarctic Strait, South Shetland Islands

1. Introduction

The amplification and propagation of the tide in the Weddell Sea and at Bransfield and Gerlache Straits (Fig. 1) has been studied by analysis of measurements (Lutjeharms *et al*., 1985; Foldvik *et al*., 1990; Speroni *et al*., 2000; D'Onofrio *et al*., 2003; Dragani *et al*., 2004). On the basis of these observational studies it is known that semidiurnal amplitudes (M_2 and S_2) around the northern extreme of the Antarctic Peninsula are

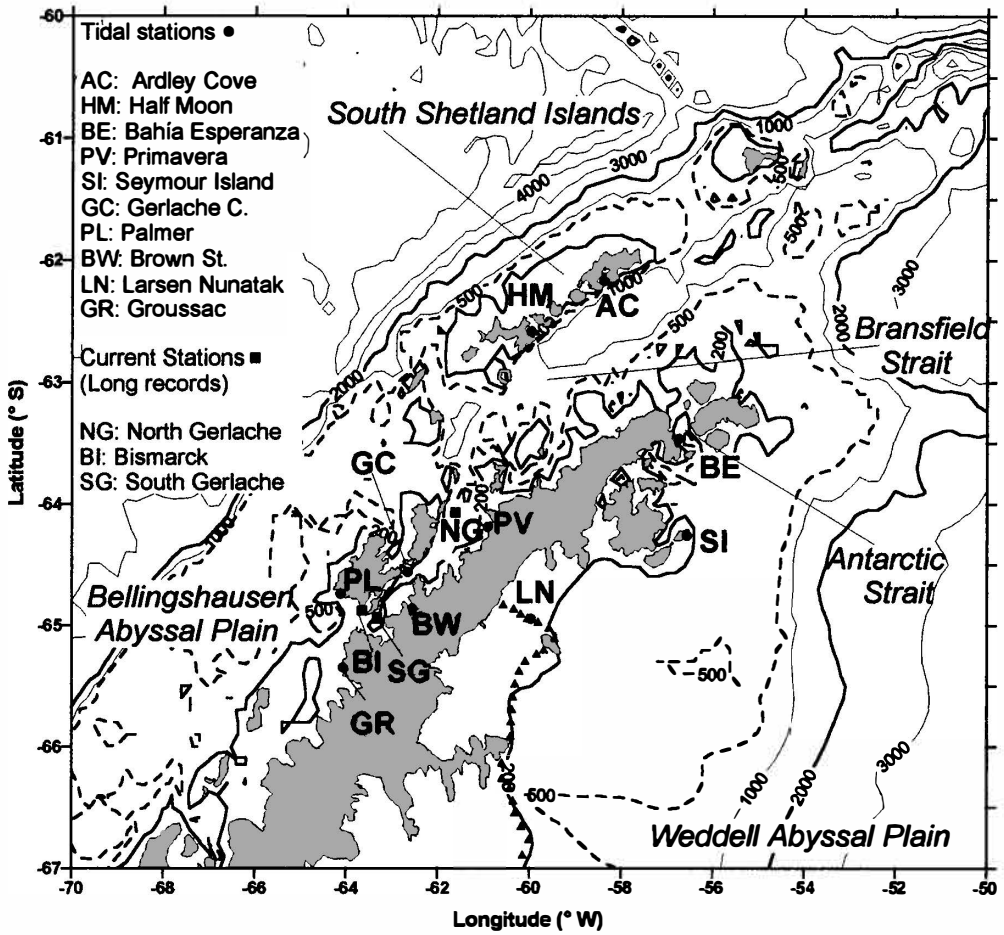

Fig. 1. Map of the study area showing the location of the tidal gauge and current meter stations used for model validation. Bathymetry from GEBCO data set (isobaths in meters).

reduced gradually from Larsen Nunatak, (0.83 m and 0.55 m, respectively) in the Weddell Sea to Groussac (0.21 m and 0.20 m, respectively) south of Bismarck Strait. Diurnal amplitudes present similar features to semidiurnal amplitudes but diurnal amplitudes are significantly lower than semidiurnal ones in the Weddell Sea. Diurnal amplitudes (O_1 and K_1) are also attenuated from Larsen Nunatak (0.40 m and 0.43 m, respectively) to the southern Gerlache Strait (0.29 m and 0.32 m, respectively). On the other hand, phase differences between Brown and Primavera are 0° for the M_2 constituent, 9° for the S_2 and 4° for the O_1 and the K_1. Such small phase differences in Gerlache Strait suggest that the water level rises and falls almost uniformly throughout the strait. The main uncertainties are located in Bransfield Strait. In this area sea level measurements are necessary not only to obtain a realistic view of tidal propagation within the study region but also to better understand the tidal dynamics.

Regarding current records, there are very few series longer than one month and

they are generally limited to the summer season because weather conditions are extremely severe during the rest of the year. Consequently, a complete view of the tidal circulation based on observed current is not available yet.

Several numerical models (Schwidersky, 1979, 1981a, b, c; Cartwright and Ray, 1990) and interpretation of satellite altimeter data were used to obtain global features of the circulation and propagation of the main tidal constituents (Kantha, 1995; Matsumoto *et al*., 1995; Le Provost *et al*., 1998; Ray, 1999). The high-resolution semi-inverse global model presented by Egbert *et al*. (1994) gave a very realistic simulation of the tide at many regions around Antarctica. The main differences between observations and global ocean models arise in shallow water regions where inaccuracies in bottom depths can often cause errors as high as 100% (Kantha, 1995). Even though such global tidal models give very good results for the deep ocean, they do not have enough resolution to describe the dynamics in shelf areas close to the coast. Matsumoto *et al*. (1995) pointed out that some problems arise in some specific areas, mainly shallow water regions and steep bathymetry regions. Finally, these authors pointed out the necessity of finer resolution tide models in order to improve the hydrodynamics in shallow waters. In this sense, Robertson *et al*. (1998) implemented a high-resolution (10′ in longitude and 5′ in latitude) barotropic tidal model to predict tidal elevations and currents in the whole Weddell Sea, the northeastern Bellingshausen Sea and Drake Passage.

Even though a good amount of sea level data are available to describe the tidal propagation there are not enough current data to describe in detail either the circulation associated to the tide or the energy flux and dissipation by the bottom. In this work we implemented a bidimensional, depth-integrated, high-resolution model to study the tidal propagation at the northern tip of the Antarctica Peninsula (northwestern Weddell Sea, Bransfield and Gerlache Straits and northeastern Bellingshausen Sea). This kind of simulation not only complements the observations (in order to obtain a better picture of the tidal propagation) but also provides the currents and other derived quantities.

The aim of this work is to validate and to implement a high-resolution model in order to describe the currents and the derived quantities around the northern tip of the Antarctic Peninsula. The paper is organized as follows. In the next section (Section 2) the study region is described. In Section 3, we present sea level and current records that were used to validate the model. In Section 4, information about the implemented model is given. In Section 5, the validation of the model, the cotidal and corange charts and the current ellipse charts for the four analyses tidal constituents (M_2, S_2, O_1 and K_1) are presented. Likewise, additional quantities calculated from our simulations (energy flux and the dissipation by bottom friction) are shown. A discussion and conclusions of the results are presented in Section 6.

2. The study region

The Antarctic Peninsula is located at the northernmost extreme of the Antarctic Continent between the Bellingshausen Sea and the Weddell Sea (Fig. 1). A continental shelf on the northwestern side of the peninsula extends eastward beyond the South Shetland Islands; another continental shelf on the southeastern side of the peninsula is

wider and better defined than one on the northwestern side. Both continental shelves present abrupt continental slopes connecting to the northwestern Weddell and the northeastern Bellingshausen Abyssal Plains deeper than 3000 m. Gerlache Strait (64°30′S, 62°20′W), on the northwestern side of the peninsula, is a narrow channel about 200 km long, which runs parallel to the Peninsula. Bismarck Strait and the Schollaert Channel connect Gerlache Strait to the Bellingshausen Sea, and the canal Orléans connects Gerlache Strait to Bransfield Strait (63°S, 59°W) between the Antarctic Peninsula and the South Shetland Islands. Gerlache and Bransfield Straits are relatively deep, in some places more than 1000 m. Both straits are characterized by the presence of many little islands, bays, coves and interconnected channels.

3. Data

3.1. Tide

The locations where sea level has been measured are shown in Table 1 and Fig. 1. In the study area sea level was measured by basic tide gauges (three stations), water level recorders with pressure sensors (two stations) and visual tide staffs and levels (five stations). A complete description of this data set was presented in D'Onofrio *et al*. (2003) and Dragani *et al*. (2004). For validation we have only used those records whose durations were equal to or longer than one month. In this work, observed data and modeled results were processed according to Foreman (1977) to obtain the tidal harmonic constants. In Table 1, observed and modeled amplitudes and Greenwich phases (Schureman, 1988) of the principal diurnal tides (O_1 and K_1) and semidiurnal tides (M_2 and S_2) are presented.

Table 1. List of locations where measurements of sea level were compared with model results. is the observed amplitudes and Greenwich phase of the tidal constituent, respectively, and F: Floater, P: Pressure sensor.

Station (Code)	Lat. (S)	Lon. (W)	Type of device	No. days	M_2			
					H_O	H_M	G_O	G_M
Ardley Cove (AC)	62.217°	58.933°	VTS	44	.46	.43	276	264
Half Moon I. (HM)	62.600°	59.884°	F	38	.43	.42	281	263
Bahía Esperanza (BE)	63.383°	56.983°	F	547	.63	.56	275	259
Primavera (PV)	64.150°	60.950°	VTS	44	.33	.36	291	259
Seymour Island (SI)	64.235°	56.575°	VTS	32	.71	.64	266	255
Gerlache C (GC)	64.593°	62.890°	P	29	.29	.33	291	257
Palmer (PL)	64.772°	64.067°	P	30	.21	.26	286	252
Brown (BW)	64.900°	62.867°	F	699	.27	.31	291	256
Larsen Nunatak (LN)	64.904°	60.043°	VTS	31	.82	.76	261	252
Groussac (GR)	65.183°	64.167°	VTS	59	.21	.25	288	251

3.2. *Currents*

The circulation around the northern Antarctic Peninsula in the high frequencies (diurnal and semidiurnal bands) is mainly dominated by tide—typical tidal currents over most of the Weddell Sea are 2–10 times greater than mean flows associated with wind and thermohaline forcing (Robertson *et al*., 1998). Current data in the study area are very scarce. We have only three relatively long records measured at the western side of the Antarctic Peninsula. North Gerlache (64.15°S, 61.38°W) and Bismarck (64.84°S, 64.02°W) current records are 31 days long. In both cases instruments were located 100 m below the surface, at 300 m depth. The South Gerlache (64.93°S, 63.42°W) current record is 32 days long. In this case the current meter was located 50 m below the surface at 93 m depth. In the three cases current was measured with an Aanderaa model RCM5 current meter. In this work, observed data modeled results were processed according to Foreman (1978) to obtain the tidal current harmonic constants. In Table 2, east-west (U) and north-south (V) observed and modeled modules and the respective Greenwich phases (G^U and G^V) of the principal diurnal and semidiurnal constituents are presented. In addition we used five short current records, four of them measured in different locations within Gerlache Strait (Legal *et al*., 1995) and one in the northwestern Weddell Sea to compare our model results. A description of those short current records measured in Gerlache Strait and the Weddell Sea is presented in Table 3.

Duration of each sea level record (in days) is presented. H_O *(in m) and* G_O *(in degrees)* H_M *(in m) and* G_M *(in degrees) the modeled ones, respectively. VTS: Visual Tide Staff,*

Constituents											
S_2				O_1				K_1			
H_O	H_M	G_O	G_M	H_O	H_M	G_O	G_M	H_O	H_M	G_O	G_M
.25	.17	331	313	.29	.21	45	51	.31	.19	73	77
.24	.16	335	316	.28	.20	49	52	.28	.20	66	78
.40	.31	312	292	.40	.25	35	42	.36	.23	53	61
.26	.10	5	335	.32	.20	59	56	.31	.21	72	83
.47	.40	301	285	.42	.28	26	36	.41	.25	46	52
.22	.08	13	351	.30	.20	60	57	.32	.22	78	84
.20	.07	34	31	.29	.20	69	61	.32	.23	83	86
.20	.08	14	4	.31	.20	63	59	.33	.22	76	85
.55	.50	299	280	.40	.31	8	34	.43	.29	32	48
.20	.08	32	38	.29	.21	68	61	.32	.24	86	86

Table 2. Locations where current were measured and compared with model results. U_O and V_O (in cms^{-1}) and G_O^U and G_O^V (in degrees) are the observed modules and Greenwich phase of the east-west and north-south current component, respectively. U_M and V_M (in cm) and G_M^U and G_M^V (in degrees) the modeled ones, respectively. Harmonic amplitudes lower than 1.0 cm s^{-1} and associated phases are not included. a) North Gerlache, b) South Gerlache and c) Bismarck current stations.

Tidal const.	Station (Code) North Gerlache (GN) (a)							
	U (E-W)				V (N-S)			
	U_O cm s^{-1}	U_M cm s^{-1}	G_O^U °	G_M^U °	V_O cm s^{-1}	V_M cm s^{-1}	G_O^V °	G_M^V °
M_2	< 1.0	1.0	---	194	1.0	1.0	186	203
S_2	< 1.0	1.0	---	196	1.0	1.0	207	191
O_1	<1.0	< 1.0	---	---	1.1	< 1.0	002	---
K_1	< 1.0	< 1.0	---	---	1.1	< 1.0	001	---

Tidal const.	Station (Code) South Gerlache (GS) (b)							
	U (E-W)				V (N-S)			
	U_O cm s^{-1}	U_M cm s^{-1}	G_O^U °	G_M^U °	V_O cm s^{-1}	V_M cm s^{-1}	G_O^V °	G_M^V °
M_2	1.0	5.2	167	184	4.4	6.2	152	184
S_2	1.2	3.9	200	200	1.3	4.7	218	200
O_1	1.5	1.7	247	226	3.4	2.0	163	227
K_1	1.0	2.2	179	201	4.6	2.8	170	201

Tidal const.	Station (Code) Bismark (BI) (c)							
	U (E-W)				V (N-S)			
	U_O cm s^{-1}	U_M cm s^{-1}	G_O^U °	G_M^U °	V_O cm s^{-1}	V_M cm s^{-1}	G_O^V °	G_M^V °
M_2	< 1.0	8.0	---	182	2.5	< 1.0	048	---
S_2	< 1.0	5.0	---	206	< 1.0	< 1.0	---	---
O_1	< 1.0	2.0	---	241	3.4	< 1.0	139	---
K_1	<1.0	2.0	---	212	2.2	< 1.0	120	---

Table 3. List of locations where short current measurement records were compared with model results. Duration (in hours), latitude, longitude, instrument, and data source are presented. Instruments depths (m) and observed and model bottom depths (m) are included. Intensity (cm s^{-1}) and direction (°) of the maximum observed and model currents are shown.

Date	Latitude (°)	Longitude (°)	Instrument	Source	Depth of instrument (m)	Depth for observation (m)	Depth for model (m)	Record length (hours)	Maximun observed (cm s^{-1}, °)	Maximun modeled (cm s^{-1}, °)
02/05-06/91	64.83	63.00	KSK	Legal *et al.* 1995	30	320	124	25	14, 321	14, 260
02/03-04/91	64.90	63.08	KSK	Legal *et al.* 1995	30	123	144	25	56, 101	13, 080
01/20-21/91	64.83	62.9	KSK	Legal *et al.* 1995	30	180	210	25	15, 346	8, 020
01/24-25/91	64.82	62.87	KSK	Legal *et al.* 1995	30	90	200	25	34, 026	7, 030
01/27-31/01	64.84	64.02	S4	D'Onofrio *et al.* 2003	6	12	100	114	84, 012	24, 010

4. Model setup

4.1. Model description

The model used for the numerical investigations is WQMap version 5.0 (Water Quality Mapping), developed by Applied Science Associates Inc. (2004). The mathematical description of tide-driven currents requires the simultaneous solution of the dynamic equations of motion and the continuity equation. If it is assumed that vertical accelerations are negligible, pressures are hydrostatic over depth, and fluid density is everywhere homogeneous, the two-dimensional, depth-averaged nonlinear equations can be written as follows:

$$\frac{\partial \eta}{\partial t}+\frac{\partial U(\eta+h)}{\partial x}+\frac{\partial V(\eta+h)}{\partial y}=0, \tag{1}$$

$$\frac{\partial U}{\partial t}+U\frac{\partial U}{\partial x}+V\frac{\partial U}{\partial y}-fV=-g\frac{\partial \eta}{\partial x}-\frac{\tau_{bx}}{\rho(h+\eta)}+A_H\nabla^2 U, \tag{2}$$

$$\frac{\partial V}{\partial t}+U\frac{\partial V}{\partial x}+V\frac{\partial V}{\partial y}+fU=-g\frac{\partial \eta}{\partial y}-\frac{\tau_{by}}{\rho(h+\eta)}+A_H\nabla^2 V, \tag{3}$$

where U and V are the mean vertically-averaged velocities in the x (E-W) and y (N-S) directions, τ_{bx} and τ_{by} are the x and y components of the bottom shear stress, A_H is the horizontal eddy viscosity coefficient, η is the free surface elevation above mean water level, h is the bottom depth below mean water level, ρ is the sea water density (constant, equal to 1028 kg m^{-3}), g is the acceleration due to gravity, f is the Coriolis parameter, ∇^2 is the horizontal Laplacian operator, and t is the time.

The two-dimensional vertically averaged equations of motion and continuity are solved using a semi-implicit method (Madala and Piacsek, 1977) in which the surface elevation is solved implicitly while the other terms in the equation such as the Coriolis, bottom stress and advective terms are solved explicitly. The momentum equations are substituted into the continuity equation to obtain a Helmholtz equation in terms of surface elevation. The spatial discretization is based on a staggered grid system (Arakawa and Lamb, 1977). Time is discretized using a three level scheme with a

weighting factor of 1.5 (Kinnmark, 1985). Thus the numerical discretization scheme used is second order accurate in space and time. The discretized Helmholtz equation is solved using a sparse matrix method to obtain the surface elevation. The vertically averaged velocities are then obtained from the vertically averaged momentum equations, using the new surface elevation.

The bottom stress is parameterized by means of a quadratic law in terms of the depth averaged current velocity:

$$\vec{\tau}_b = (\tau_{bx}, \tau_{by}) = C_b \rho \vec{V} |\vec{V}|, \tag{4}$$

where C_b is the nondimensional drag or bottom friction coefficient. In order to test model sensitivity to C_b, different experiments using values of C_b ranging from 0.002 to 0.004 were done. Since the solutions do not exhibit significant sensitivity to C_b, a constant value equal to 0.003 was selected for the solutions shown in this paper. $\vec{V}$ is the mean averaged depth current whose east-west and north-south components are U and V, respectively.

The model domain includes the northwestern Weddell Sea, the northeastern Bellingshausen Sea and the adjacent continental shelves (Fig. 1). The model spans the region between 60°S and 67°S, and 50°W and 70°W, approximately. We did some numerical experiments using bathymetry digitized from the nautical chart H-7 (SHN, 1997) but the results obtained showed that this data set was not appropriate because depths, especially around the South Shetland Islands, are underestimated. Then, we performed some numerical experiments with bathymetry taken from the ETOPO2 data base (National Geophysical Data Center, 1992) but the results were also unsatisfactory. Finally, validation indicates that the solution obtained with a $1' \times 1'$ resolution depth data set coming from GEBCO (2003) provides results which presented the lowest differences between observed and model harmonic constants. Numerical experiments were done using a grid with 2.43×1.94 km ($3.00' \times 1.05'$) resolution with 400×400 grid points in the east-west and north-south directions, respectively. This grid was created from a $1' \times 1'$ resolution GEBCO data set, using the method of inverse distance to the power (with power equal to 2).

4.2. Initial and boundary conditions

The model is initially at rest, *i.e.* U, V, and η are zero everywhere. Model forcing was introduced by imposing tidal elevation at the open boundaries using the classical tidal description of sea level,

$$\eta(t) = Z_o + \sum_{n=1}^{4} H_n \cos(\omega_n t + \phi_n - G_n), \tag{5}$$

where $\eta(t)$ is the tidal level at time t, Z_o the height of the mean water level, and H_n, G_n, ω_n and ϕ_n are the amplitude, Greenwich phase lag, angular speed and equilibrium phase of the four main constituents (M_2, S_2, K_1 and O_1) which were used to obtain the tidal level at every grid point on the open boundary. Amplitudes and phases derived from the Oregon State University (OSU) global model (Egbert *et al*., 1994) were used to force the model. A bilinear interpolation routine was used to convert OSU (0.58° in latitude and 0.70° in longitude) resolution model outputs into amplitudes and phases at

$3.00' \times 1.05'$ resolution at the boundaries of the model. The model was spun up by increasing the tidal forcing linearly from zero over one day. The simulation time step for the model was 7.5 s. With this relatively small time step, stability and absence of numerical damping and phase lags, which may occur at long time steps, are ensured.

Modeling the tide and tidal currents within the computational domain required specification of the current velocities along the open boundaries. Because these velocities were not known accurately enough to be assigned to the model, the values of U and V at the boundary were set equal to their values at the first interior point. This represents the null gradient radiation condition (Chapman, 1985). Along closed boundaries the normal component of the current was set to zero and a free slip boundary condition was assumed.

The model was run for the equivalent of 32 days. After approximately 1.5 days of simulation most of the transients due to the spin up of the model are dissipated. Consequently, in order to ensure the stability of the solution the analysis was done by using only the last 30 days of the simulation with hourly data.

5. Results

5.1. Tidal levels

Cotidal and corange charts corresponding to the M_2, S_2, K_1 and O_1 tidal components obtained by harmonic analysis from the numerical simulation performed with the model are shown in Fig. 2. With regard to the M_2 amplitude (Fig. 2), the highest values occur in the northwestern Weddell Sea. These amplitudes decrease gradually around the peninsula, from Larsen Nunatak (0.7 m) to the southwestern corner of the modeled area (0.2 m). M_2 amplitudes present a relative maximum around the South Shetland Islands (0.45 m). M_2 Greenwich phases present weak spatial variability in the study area, ranging from 240° to 270°. The M_2 tidal wave propagates northeastward both at the northwestern Weddell Sea and the northwestern side of the Antarctic Peninsula. S_2 corange lines also decrease gradually around the Antarctic Peninsula, from 0.6 m in the Weddell Sea to 0.1 m in the northeastern Bellingshausen Sea (Fig. 2). In contrast, S_2 cotidal lines present a gyre around the Antarctic Peninsula from Weddell Sea to Bellingshausen Sea.

Diurnal (K_1 and O_1) cotidal and corange lines present similar characteristics. Amplitudes are very alike in the study area. They are only 0.1 m greater on the northeastern side than on the northwestern side of the peninsula. K_1 and O_1 tidal waves turn around the peninsula from the Weddell Sea to the Bellingshausen Sea.

Table 1 shows a comparison between observed and modeled amplitudes and phases at the locations shown in Fig. 1. In order to simplify the interpretation of the results, Fig. 3 displays scatter plots of the modeled and observed values of amplitude and phase for the four analyzed tidal constituents. The dashed line represents the ideal fit and the determination coefficient is also included in each case. Table 1 and Fig. 3 indicate that, in general, the model is in good agreement with observations. The agreement between M_2 observed and modeled amplitudes is very good but the agreement between phases is rather poor. As can be seen in Table 1, our results slightly underestimate the observations in the Gerlache Strait area by approximately 30°. In contrast, we have obtained

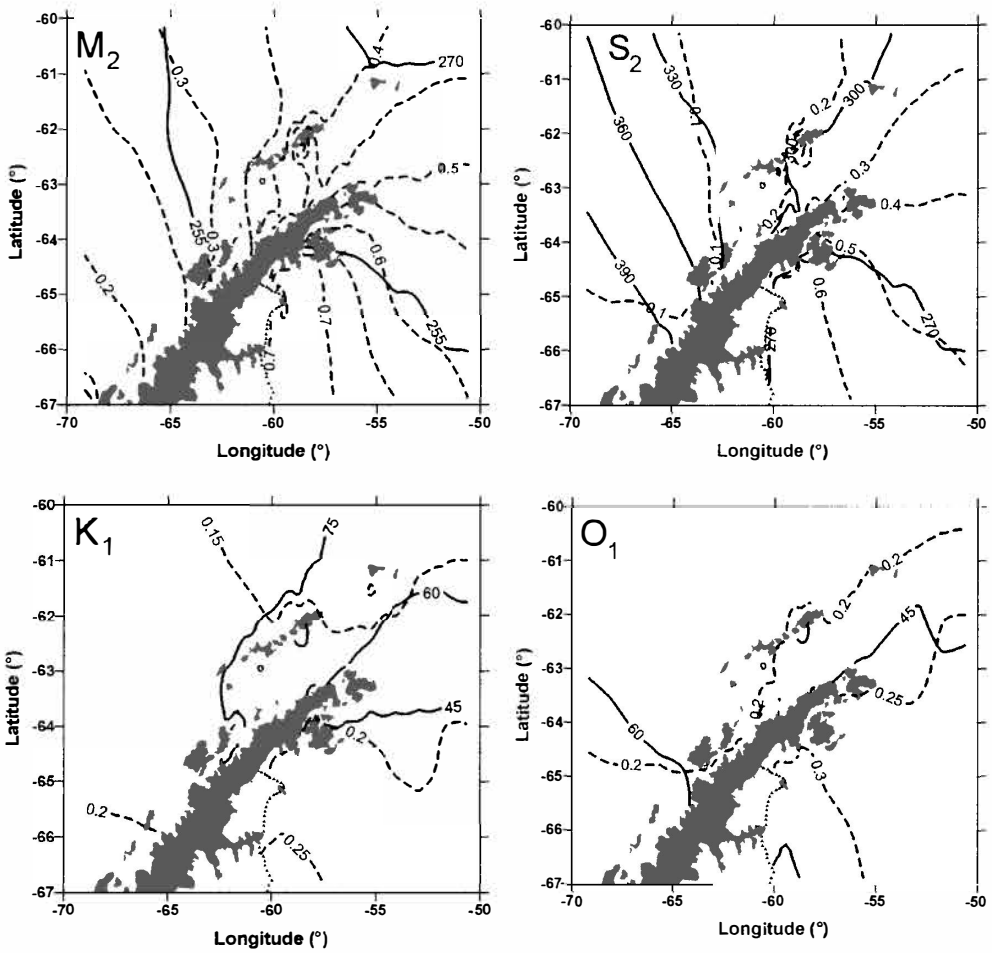

Fig. 2. Corange (solid lines, amplitudes in meters) and cotidal (dashed lines, Greenwich phases in degrees) maps for the M_2, S_2, K_1 and O_1 tidal constituents, derived from WQMap model.

better agreement in the northwestern Weddell Sea, at Seymour Island and Nunatak Larsen stations. S_2 modeled amplitudes are also slightly underestimated, especially in Gerlache Strait, but in general, the agreement between observations and results is good. S_2 modeled phases are in good agreement with the observations. The major differences can also be appreciated in Bransfield Strait (approximately 20°) at Half Moon and Ardley Cove stations. Modeled diurnal amplitudes are lightly lower than observations by approximately 0.10–0.15 m. Modeled diurnal phases agree very well with the observations. Differences between observed and modeled phases are, in general, lower than 12°. The exception is Larsen Nunatak station, where O_1 and K_1 observed phases are 26° and 16° lower than the modeled ones, respectively.

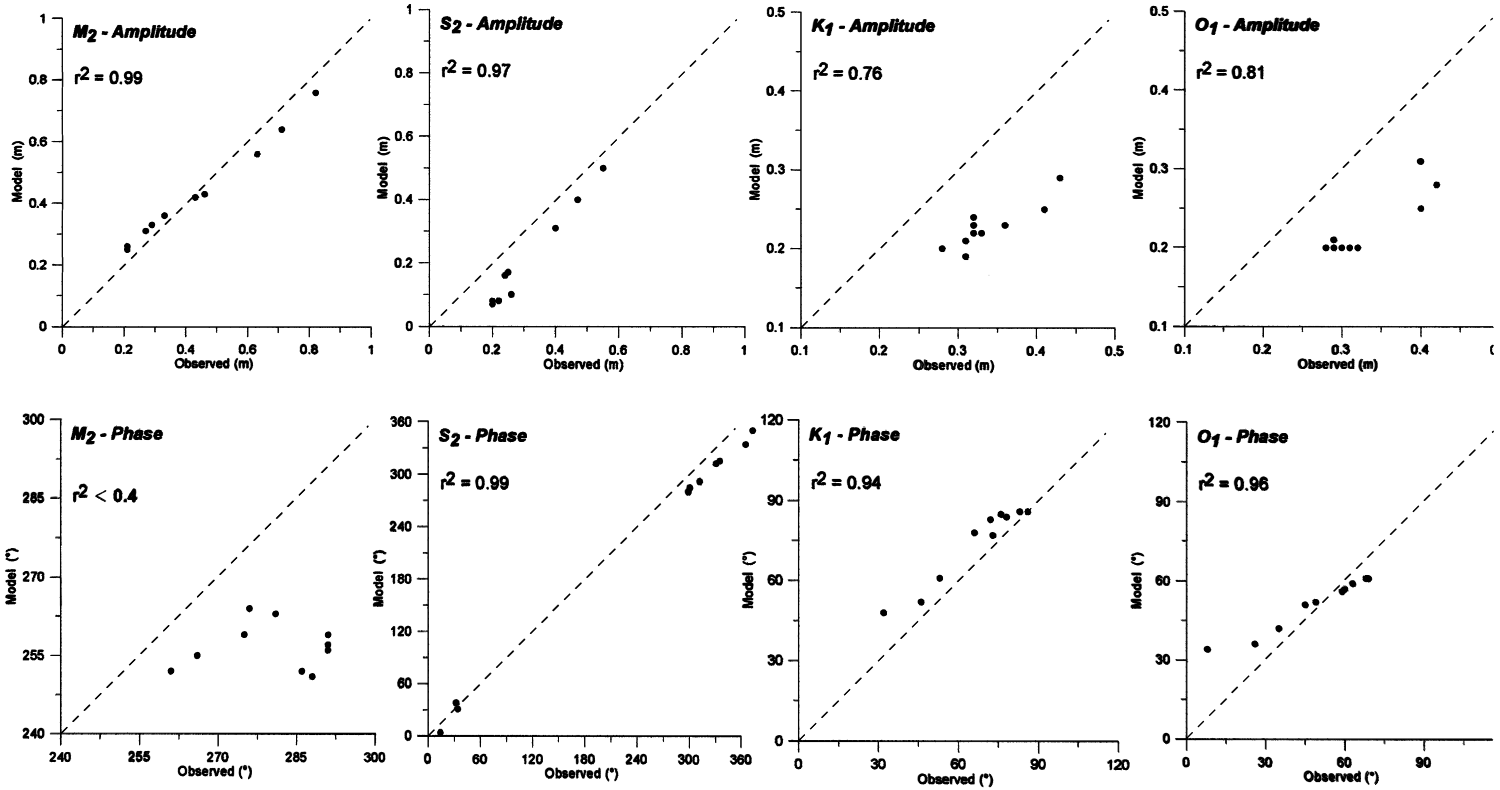

Fig. 3. Scatter plots of modeled vs. observed amplitudes (upper panel) and phases (lower panel) for the M_2, S_2, K_1 and O_1 tidal constituents. Dashed line indicates the perfect fit.

5.2. *Tidal currents*

In order to validate the currents resulting from the simulations, harmonic constants obtained from model results were compared with constants calculated from data records whose characteristics are given in Table 2. These current stations were located in Gerlache Strait. Observations indicate that tidal currents are noticeably low at North Gerlache (NG) and at Bismark Strait (BI) stations, and the simulations properly reproduce this fact. Phases are satisfactorily reproduced at South Gerlache station (SG), but the model tends to overestimate the speeds for the M_2 and S_2 constituents. Observed and modeled amplitudes are lower or equal than $0.01\,\mathrm{ms}^{-1}$ at NG station. The model slightly overestimates the east-west amplitudes and underestimates the north-south amplitudes at BI station. Harmonic constants corresponding to component amplitudes lower than $0.01\,\mathrm{ms}^{-1}$ are not included in Table 2 because they are below the threshold of the instrument. A comparison between maximum speeds obtained from short records and the maximum speed for the 30 day-long simulation is presented in Table 3. Four stations were located in Gerlache Strait and one in the northwestern Weddell Sea. The simulations correctly reproduce the directions of maximum speeds but underestimate the intensity. One possible cause is because our numerical experiments only included tidal forcing but not meteorological effects.

Modeled tidal ellipse axes for each tidal harmonic constant are shown in Fig. 4. Largest currents are observed at narrow channels between islands (for instance South Shetland Islands, Fig. 1) and in the Antarctic Strait. Semidiurnal tidal currents (M_2 and S_2) present a similar pattern (Fig. 4). The highest currents appear in narrow channels among islands and the current is relatively low in the northwestern Weddell Sea and northeastern Bellingshausen Sea. In these regions the major axes are oriented parallel to the peninsula and the current is preponderantly unidirectional. At the eastern of the tip of the Antarctic Peninsula major axes are oriented in the east-west direction. This responds to the fact that the bottom bathymetry presents a submarine ridge with a very significant gradient and, consequently, the averaged depth integrated velocities are oriented following the bottom contour directions. In Gerlache Strait, tidal currents are weakened, possibly because this strait is very deep and is connected with the Bellingshausen Sea and Bransfield Strait through relatively narrow channels. Diurnal tidal ellipse' patterns (K_1 and O_1) are comparable to semidiurnal ones, but the major axes are slightly lower than the semidiurnal major axes (Fig. 4).

5.3. *Tidal energetics*

Additional important quantities that can be calculated from our simulations are the energy flux and dissipation by bottom friction. Given the good correspondence between simulated and observed harmonic constants of sea level and tidal currents, it is expected that a good estimation of these quantities will derive from model results. The energy flux can be computed as (Robertson *et al*., 1998):

$$F_x = \frac{1}{2}\rho g h U_{\mathrm{M}} H_{\mathrm{M}} \cos(G_{\mathrm{M}} - G_{\mathrm{M}}^{U}), \tag{6}$$

$$F_y = \frac{1}{2}\rho g h V_{\mathrm{M}} H_{\mathrm{M}} \cos(G_{\mathrm{M}} - G_{\mathrm{M}}^{V}), \tag{7}$$

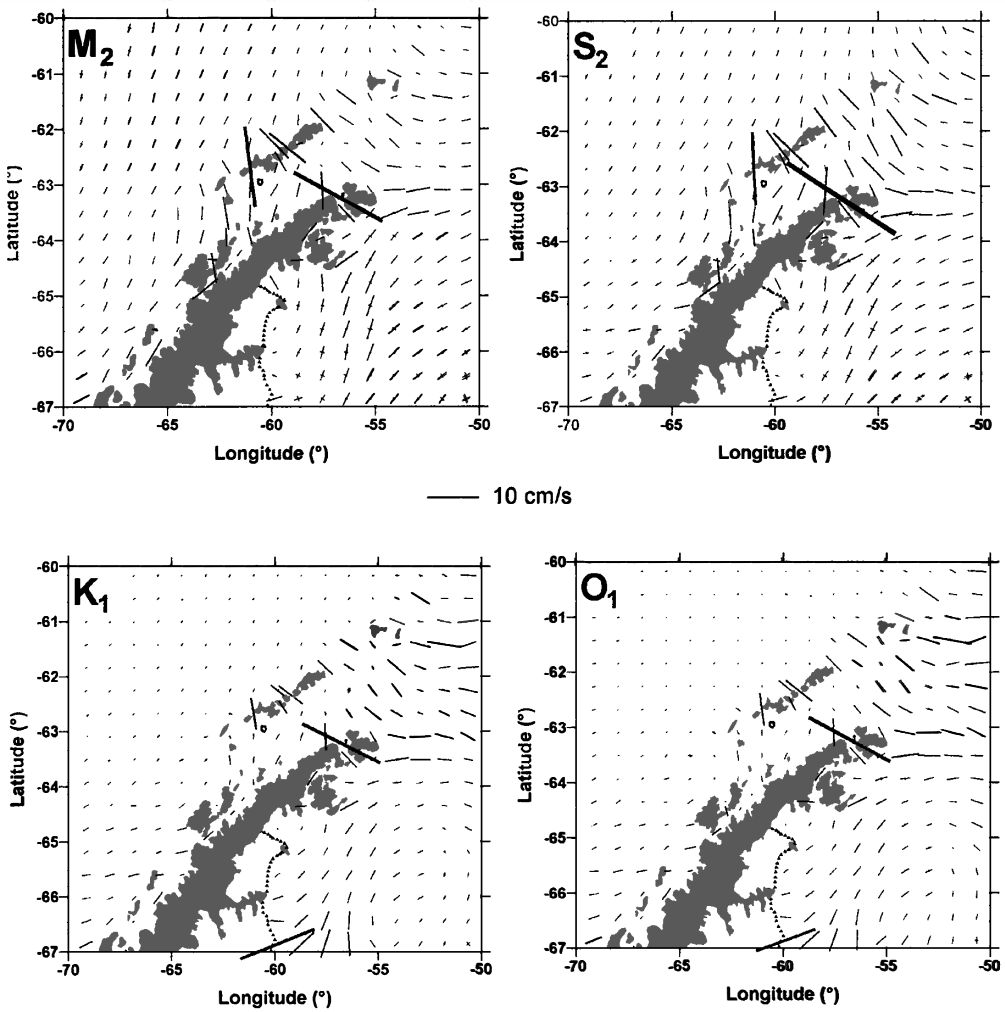

Fig. 4. M_2, S_2, K_1 and O_1 tidal current ellipses derived from the model.

where F_x and F_y are the x and y components of the energy flux vector, respectively, H_M is the modeled amplitude of the elevation and G_M its Greenwich phase. (U_M, V_M) and (G_M^U, G_M^V) are the amplitude and the Greenwich phase of the vertically averaged current components in the zonal and meridional directions respectively, calculated from harmonic analysis of the time series derived from the model.

M_2 and S_2 energy fluxes computed with harmonic constants obtained in this work present very similar characteristics (Fig. 5). In both cases the energy flux turns around the peninsula from the Weddell Sea to the Bellingshausen Sea; the highest values are present in the Weddell Sea and the energy flux shows a relative maximum in the Antarctic Strait flowing from the Weddell Sea to Bransfield Strait. Northward the Bellingshausen Sea M_2 and S_2 energy flux is southwestward, the intensity of the M_2 flux

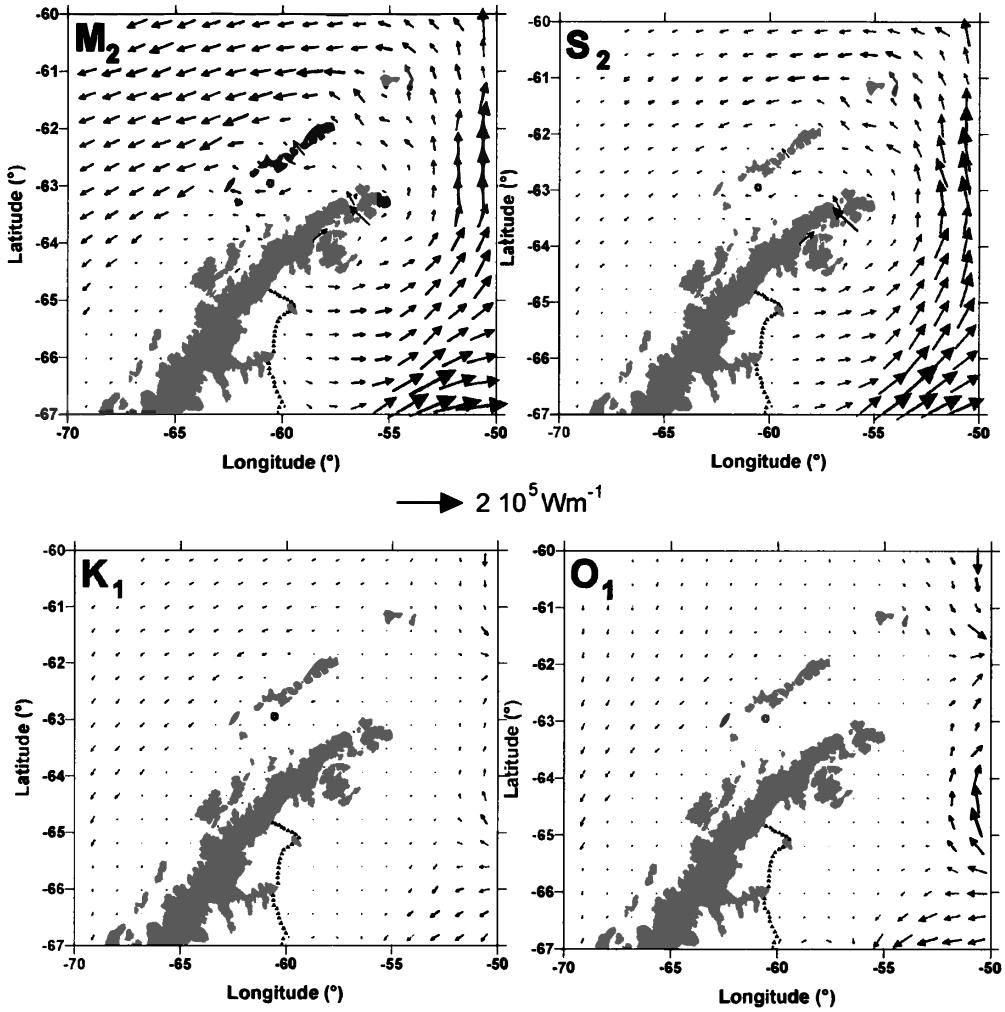

Fig. 5. M_2, S_2, K_1 *and* O_1 *tidal energy flux vectors in* $W\ m^{-1}$.

being higher than the S_2 one. On the northwestern side of the peninsula, O_1 and K_1 energy fluxes are very similar to the semidiurnal ones in direction but they are significantly lower in magnitude (Fig. 5). In the northwestern Weddell Sea the O_1 and K_1 flux magnitudes are very low, showing an eastward gradual increase and a significant variability in direction.

Tidal energy in the real ocean is dissipated by several mechanisms, including bottom friction, lateral friction, friction between the pack ice and the water, topographic drag and flexure of the ice shelves. Our model parameterizes the first two of these sinks; however, the others are ignored. Davies *et al*. (1985) presented an expression for evaluating the time-averaged dissipation of energy per unit area by bottom friction, given by:

$$D_b = \frac{1}{T} c_b \rho \int_0^T (U^2 + V^2)^{3/2} \, dt, \tag{8}$$

where the integration period T was 30 days. We used this equation in order to identify the most important areas for dissipation of energy and quantify its value in the modeled area. The result is presented in Fig. 6. The energy lost in the deep water of the northwestern Weddell and northeastern Bellingshausen Seas is small, since velocities are small throughout these regions. Nearly all the dissipation occurs in the Antarctic Strait (maximum value ~0.25 Wm^{-2}) and around the South Shetland Islands. The total tidal energy lost to bottom friction in our 4-constituent model is about 1.5 GW, giving a domain-averaged value of ~0.002 Wm^{-2}.

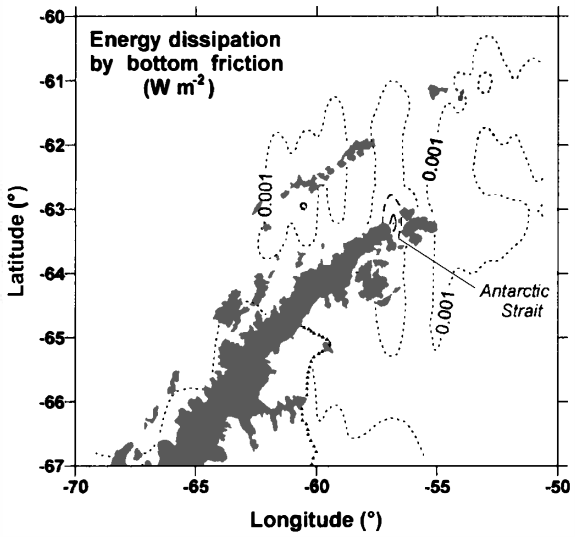

Fig. 6. Tidal energy dissipation by bottom friction rate in Wm^{-2}. Dotted line is 0.001 Wm^{-2}. At the Antarctic Strait, dashed line is 0.1 and solid line is 0.2 Wm^{-2}, respectively.

6. Discussion and conclusions

The patterns of the cotidal and corange lines resulting from our model are similar to those obtained by Robertson *et al*. (1998) who used a high-resolution barotropic tidal model. Likewise, they are very similar to the cotidal and corange lines obtained by Dragani *et al*. (2004) based in direct observations on the northwestern side of the Antarctica Peninsula. The main differences can be seen in the M_2 cotidal chart on the western side of the peninsula: although the propagation of the M_2 tidal wave (Fig. 2) is similar to those given by Robertson *et al*. (1998) and Dragani *et al*. (2004), the 270° cotidal line parallel to the peninsula in Bransfield and Gerlache Straits is not present in our results. Model phases obtained in this paper are slightly lower than the observed phases in the Gerlache Strait area (approximately 30°). In contrast, we have obtained better agreement in the northwestern Weddell Sea, at Seymour Island and Larsen

Nunatak stations.

Tidal currents are very low at the locations where we have relatively long data records. Even though our model reproduces the main characteristics of the tidal currents, we detected some differences between observed and modeled currents. A possible reason that explains these differences is due to U and V components are computed in every node of a staggered grid system that quite often can differ from the actual depth at the site of observation by as much as 20%.

Modeled tidal ellipse axes are shown in Fig. 4. The largest currents are observed in narrow channels between islands (South Shetland Islands) and in Antarctic Strait. Although we have no current data to validate the aforementioned results, information obtained during Summer Antarctic Campaigns based on visual ice drift observations confirm that large tidal currents characterize these areas.

Robertson *et al*. (1998) concluded that on the northwestern side of the Antarctic Peninsula M_2 energy flux propagates northeastward, and in the northwestern Weddell Sea energy flux is southward, close to the peninsula, and northward, more to the east. On the another hand, O_1 flux energy computed by Robertson *et al*. (1998) is southwestward on the northwestern side of the peninsula (practically in the opposite direction that the M_2 flux) but in the northwestern Weddell Sea M_2 and O_1 fluxes present similar characteristics. Our results are qualitatively similar to those derived by Robertson *et al.* (1998). The main difference can be seen in the M_2 flux, on the northwestern side of the peninsula. While results obtained by Robertson *et al*. (1998) indicated a predominantly northeastward flux, M_2 energy flux computed in this paper is southwestward. In contrast, the O_1 energy flux computed in this work is in good agreement with the Robertson *et al*. (1998) results.

Finally, although we have good sea level data records on the northwestern side of the Antarctica Peninsula, the main uncertainties raised in our model are located in Gerlache Strait, where complementary long sea level measurements would be necessary to obtain a realistic view of tidal propagation within the study region. Likewise, there are not enough current observations in Antarctic Strait, where a maximum of energy lost by bottom friction and a very significant semidiurnal energy flux, from the Weddell Sea to the Bransfield Strait, were determined in our study.

Acknowledgments

The project "Prevención de la Contaminación Costera y Gestion de la Biodiversidad Biológica Marina, SayDS—Donación fmam nro. 28385—AR—PNUD ARG/02/018" allowed the use of the WQMap model.

References

Applied Science Associates Inc. (2004): Wqmap User Manual (version 5.0). Applied Sci. Assoc., Narragansett, RI, US, 76 p.

Arakawa, A. and Lamb, V.R. (1977): Computational design of the basic dynamical processes of the UCLA General Circulation Model. Method Comput. Phys., **17**, 173–165.

Cartwright, D.E. and Ray, R.D. (1990): Oceanic tides from Geosat Altimetry. J. Geophys. Res., **96**, 16897–16912.

Chapman, D.C. (1985): Numerical treatment of cross-shelf open boundaries in a barotropic coastal ocean model. J. Phys. Oceanogr., **15**, 1060–1075.

Davies, A.M., Sauvel, J. and Evans, J. (1985): Computing near coastal tide dynamics from observations and a numerical model. Cont. Shelf Res., **4**, 341–366.

D'Onofrio, E.E., Dragani, W.C., Speroni, J.O. and Fiore, M.E. (2003): Propagation and amplification of tide at the northwestern coast of the Antarctic Peninsula: an observational study. Polar Geosci., **16**, 53–60.

Dragani, W.C., Drabble, M.R., D'Onofrio, E.E. and Mazio, C.A. (2004): Propagation and amplification of tide at the Bransfield and Gerlache Straits, northwestern Antarctic Peninsula. Polar Geosci., **17**, 156–170.

Egbert, G.D., Bennett, A.F. and Foreman, M.G.G. (1994): TOPEX/POSEIDON tides estimated using a global inverse model. J. Geophys. Res., **99**, 24821–24852.

Foldvik, A., Middleton, J.H. and Foster, T.D. (1990): The tides of the southern Weddell Sea. Deep-Sea Res., part A, **37**, 1345–1362.

Foreman, M.G.G. (1977): Manual for tidal heights analysis and prediction. Pac. Mar. Sci. Rep., **77**–**10**, 58 p.

Foreman, M.G.G. (1978): Manual for tidal currents analysis and prediction. Pac. Mar. Sci. Rep., **78**–**6**, 57 p.

GEBCO (2003): User Guide to the Centenary Edition of the GEBCO Digital Atlas and Its Data Sets, ed. by M.T. Jones. Natural Environment Research Council, 141 p.

Kantha, L.H. (1995): Barotropic Tides in the Global Oceans from a Nonlinear Tidal Model Assimilating altimetric tides. 1. Model description and results. J. Geophys. Res., **100**, 25283–25308.

Kinnmark, I. (1985): The Shallow Water Equations; Formulation, Analysis and Application. New York, Springer.

Legal, N., D'Onofrio, E. and Mazio C. (1995): Dinámica de marea y corriente en el sector oeste de la Península Antártica. Servicio de Hidrografia Naval de la Armada Argentina, Tech. Rep. 92.

Le Provost, C., Lyard, F., Molines, J.M., Genco, M.L. and Rabilloud, F. (1998): A hydrodynamic ocean tide model improved by assimilating a satellite altimeter-derived data set. J. Geophys. Res., **103**, 5513–5529.

Lutjeharms, J.R.E., Stavropoulos, C.C. and Koltermann, K.P. (1985): Tidal measurements along the Antarctic Coastline. Oceanology of the Antarctic Continental Shelf. Washington, D.C., Am. Geophys. Union, 273–289 (Antarct. Res. Ser., **43**).

Madala, R.V. and Piacsek, S.A. (1977): A semi-implicit numerical model for baroclinic ocean. J. Comp. Phys., **23**, 167–178.

Matsumoto, K., Ooe, M., Sato T. and Segawa J. (1995): Ocean tide model obtained from Topex/Poseidon altimetry data. J. Geophys. Res., **100**, 25319–25330.

National Geophysical Data Center (1992): GEODAS CD-ROM worldwide marine geophysical data, Data Announce, 92-MGG-02. Natl. Oceanic and Atmos. Admin. U.S. Dep. Commer., Boulder, Colorado.

Ray, R. (1999): A global ocean tide model from T/P altimetry: GOT99.2 NASA Technical Memorandum, NASA/TM-1999-209478, National Aeronautics and Space Administration, Goddard Space Flight Center, Greenbelt, MD.

Robertson, R.A., Padman, A.L. and Egbert, G.D. (1998): Tides in the Weddell Sea. Ocean, Ice and Atmosphere: Interactions at the Antarctic Continental Margin, ed. by S.S. Jacobs and R.F. Weiss. Washington, D.C., Am. Geophys. Union, 341–369 (Antarct. Res. Ser., 75).

Schureman, P. (1988): Manual of Harmonic Analysis and Prediction of Tides. Washington, U.S. Government Printing Office, Special Publ. N° **98**, 317 p.

Schwiderski, E.W. (1979): Global ocean tides, Part II: the semidiurnal principal lunar tide (M_2), atlas of tidal charts and maps. Dahlgen, Naval Surface Weapons Center, NSWC TR 79–414.

Schwiderski, E.W. (1981a): Global ocean tides, Part III: the semidiurnal principal solar tide (S_2), atlas of tidal charts and maps. Dahlgen, Naval Surface Weapons Center, NSWC TR 81–122.

Schwiderski, E.W. (1981b): Global ocean tides, Part IV: the diurnal luni-solar declination tide (K_1), atlas of tidal charts and maps. Dahlgen, Naval Surface Weapons Center, NSWC TR 81–142.

Schwiderski, E.W. (1981c): Global ocean tides, Part V: the diurnal principal lunar tide (O_1), atlas of tidal charts and maps. Dahlgen, Naval Surface Weapons Center, NSWC TR 81–142.

SHN (1997): Península Antártica. Carta Náutica H-7 (1: 1500000). Servicio de Hidrografia Naval, Armada

Argentina.
Speroni, J.O., Dragani W.C., D'Onofrio E.E., Drabble M.R. and Mazio C.A. (2000): Estudio de la marea en el borde de la barrera Larsen, Mar de Weddell noroccidental. Geoacta, **25**, 1–11.